FSUE Russian Federal Nuclear Center – Zababakhin All-Russia Research Institute of Technical Physics

"ROSATOM" STATE CORPORATION

Comparison of two image reconstruction algorithms for early-photon fluorescence molecular tomography

Alexander B. Konovalov

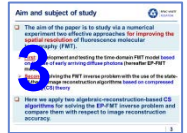*Vitaly V. Vlasov*

Alexander S. Uglov

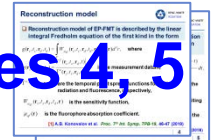**SFM 2020**
Internet Biophotonics XIII
Saratov, Oct 01 2020

Contents

Aim and subject of study
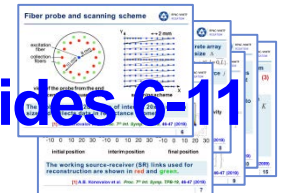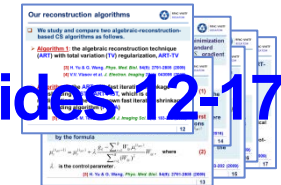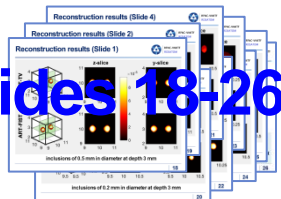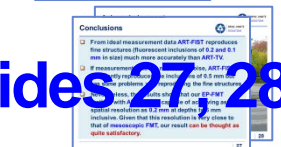
❑ **The aim of the paper is to study via a numerical experiment two effective approaches for improving the spatial resolution of fluorescence molecular tomography (FMT).**

➢ <u>First</u>**: Development and testing of the time-domain FMT model based on the use of early arriving diffuse photons (hereafter EP-FMT model)**

➢ <u>Second</u>**: Solving the FMT inverse problem with the use of the state-of-the-art image reconstruction algorithms based on compressed sensing (CS) theory**

❑ **Here we apply two algebraic-reconstruction-based CS algorithms for solving the EP-FMT inverse problem and compare them with respect to image reconstruction accuracy.**

Reconstruction model

❑ **Reconstruction model of EP-FMT is described by the linear integral Fredholm equation of the first kind in the form**

$$g(\mathbf{r}_s, t_s, \mathbf{r}_d, t_d) = \int\limits_V W_{\mu_{af}}(\mathbf{r}_s, t_s, \mathbf{r}_d, t_d, \mathbf{r})\, \mu_{af}(\mathbf{r})\, d^3 r, \quad \textbf{where}$$

$$g(\mathbf{r}_s, t_s, \mathbf{r}_d, t_d) = \frac{\Gamma^f(\mathbf{r}_s, t_s, \mathbf{r}_d, t)\big|_{t=t_d}}{\Gamma^e(\mathbf{r}_s, t_s, \mathbf{r}_d, t)\big|_{t=t_d}} \quad \textbf{is the measurement datum,}$$

$\Gamma^{e,f}(\mathbf{r}_s, t_s, \mathbf{r}_d, t)$ **are the temporal point spread functions for exiting radiation and fluorescence, respectively,**

$W_{\mu_{af}}(\mathbf{r}_s, t_s, \mathbf{r}_d, t_d, \mathbf{r})$ **is the sensitivity function,**

$\mu_{af}(\mathbf{r})$ **is the fluorophore absorption coefficient.**

[1] A.B. Konovalov et al. *Proc. 7th Int. Symp. TPB-19,* **46-47 (2019)**

4

Sensitivity function

❑ **The sensitivity function responsible for the reconstruction of the fluorophore absorption coefficient is written in the form**

$$W_{\mu_{af}}(\mathbf{r}_s, t_s, \mathbf{r}_d, t_d, \mathbf{r}) = c\gamma \int_{t_s}^{t_d} \frac{4Dct^2}{\tau |\mathbf{r}|^2 + 4Dct^2} \frac{G^e(\mathbf{r} - \mathbf{r}_s, t - t_s)\dfrac{\partial}{\partial \eta} G^e(\mathbf{r}_d - \mathbf{r}, t_d - t)}{\dfrac{\partial}{\partial \eta} G^e(\mathbf{r}_d - \mathbf{r}_s, t_d - t_s)} dt,$$

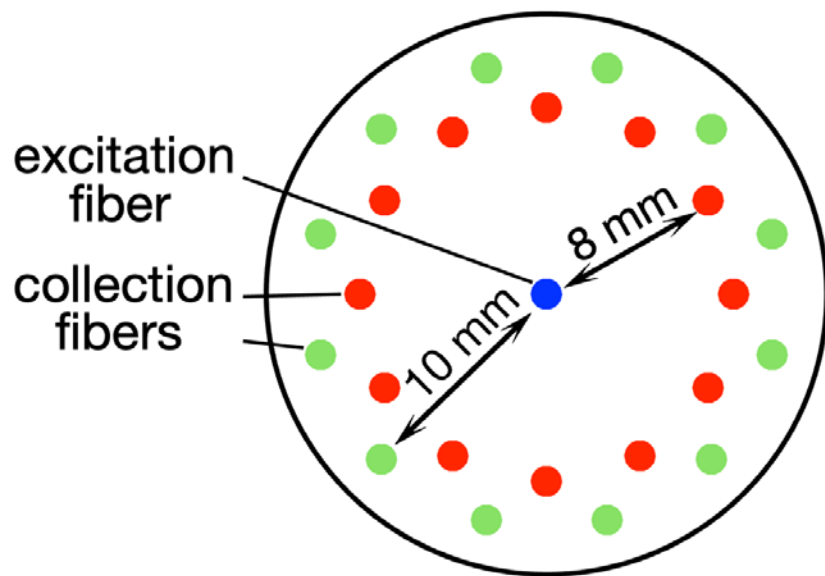c, D and γ, τ **are the optical and fluorescence parameters of the object, respectively,**

$G^e(\mathbf{r} - \mathbf{r}', t - t')$ **is the Green function of the diffusion equation for exiting radiation,**

$\partial / \partial \eta$ **is the derivative in the direction of the internal normal to the boundary at the signal registration point.**

[1] A.B. Konovalov et al. *Proc. 7th Int. Symp. TPB-19,* 46-47 (2019)

5

Fiber probe and scanning scheme

view of the probe from the end
adjacent to the mouse back
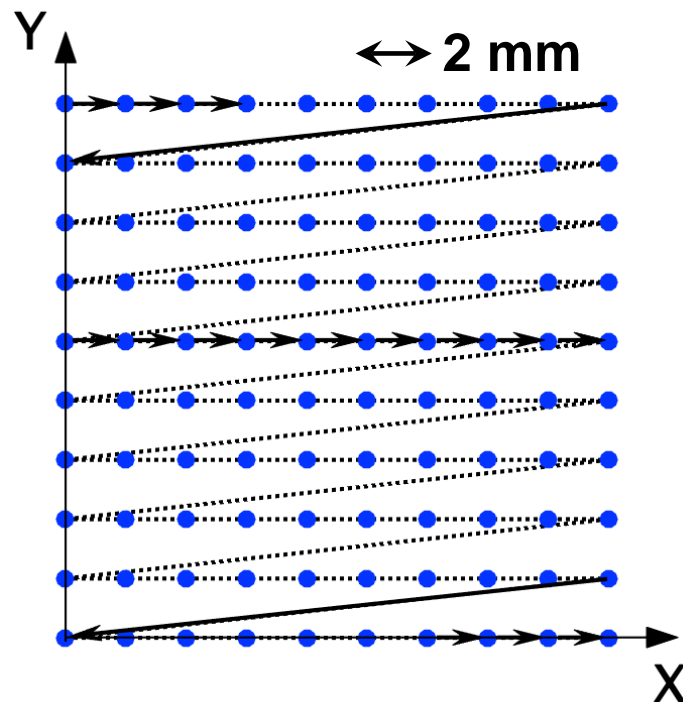
scanning scheme

The probe scans a 2D region of interest 20x20 mm² in size and collects data in reflectance geometry.

[1] A.B. Konovalov et al. *Proc. 7th Int. Symp. TPB-19,* 46-47 (2019)

Three probe positions in scanning

initial position   interim position   final position
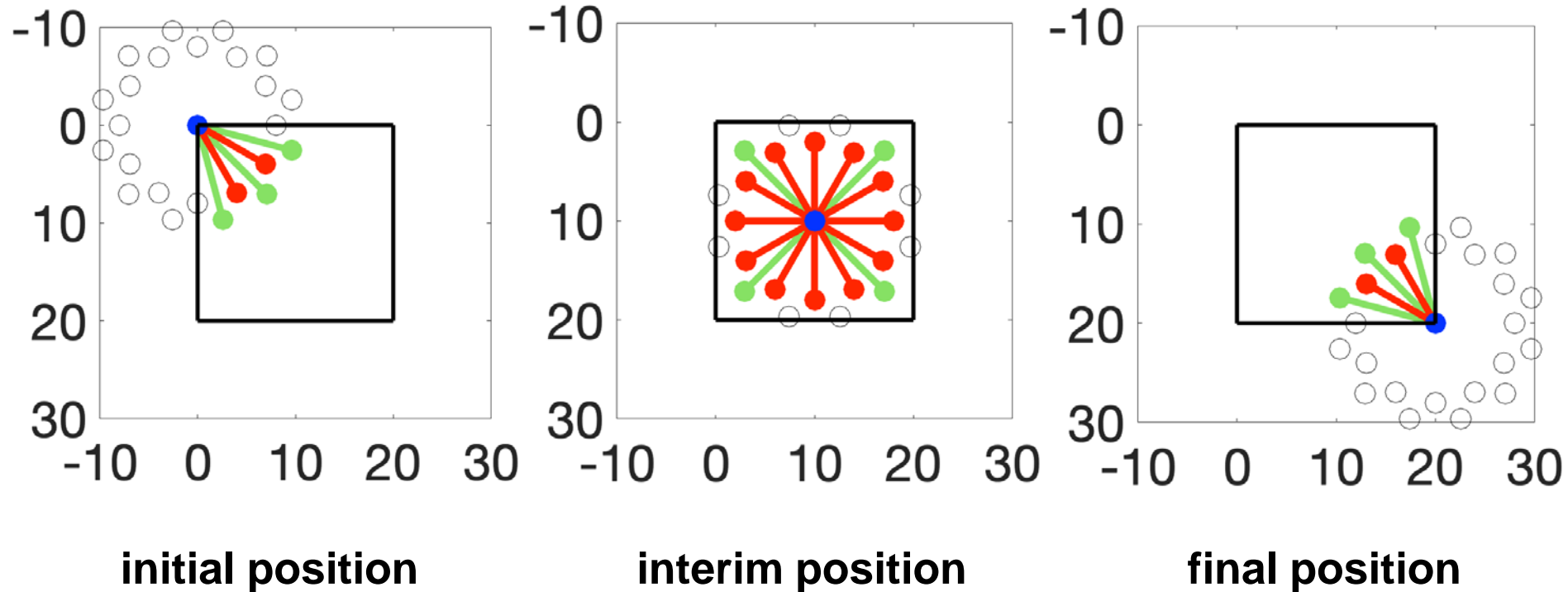
The working source-receiver (SR) links used for reconstruction are shown in red and green.

[1] A.B. Konovalov et al. *Proc. 7th Int. Symp. TPB-19,* 46-47 (2019)

7

Discretization of the Fredholm equation

Let an unknown $\mu_{af}(\mathbf{r})$ **be defined by a 3D discrete array** $\{\mu_{m,n,l}\}_{1,1,1}^{M,N,L}$ **on a Cartesian mesh of cubic cells of size** Δ

$$\{(x_n, y_m, z_l): x_n = x_0 + \Delta n, n = \overline{0,N}; y_m = y_0 + \Delta m, m = \overline{0,M}; z_l = z_0 + \Delta l, l = \overline{0,L}\}.$$

Then for the discrete measurement datum $g_{i,j}$ **for source** j **and receiver** i **we obtain**

$$g_{i,j} = \sum_{m=1}^{M}\sum_{n=1}^{N}\sum_{l=1}^{L} W_{m,n,l}^{i,j}\mu_{m,n,l}, \quad \text{where}$$

$W_{m,n,l}^{i,j}$ **is the weight coefficient that has the meaning of a sensitivity matrix element and can be presented analytically as**

$$W_{m,n,l}^{i,j} = \left(W_{m,n,l}^{i,j}\right)_{-} - \left(W_{m,n,l}^{i,j}\right)_{+}, \quad \text{where}$$

[1] A.B. Konovalov et al. *Proc. 7th Int. Symp. TPB-19,* 46-47 (2019)

$$\left(W_{m,n,l}^{i,j}\right)_{\pm} = \frac{\Delta^3 \gamma z_l}{24\pi D^{5/2}(ct_d)^{1/2}} \cdot \frac{4Dct_d^2}{\tau[(x_i - x_j)^2 + (y_i - y_j)^2 + (3D)^2] + 4Dct_d^2}$$

$$\times \exp\left[\frac{(x_i - x_j)^2 + (y_i - y_j)^2 + (3D)^2}{4Dct_d} - \left(\sqrt{\frac{(x_n - x_i)^2 + (y_m - y_i)^2 + z_l^2}{4Dct_d}}\right.\right.$$

$$\left.\left.+ \sqrt{\frac{(x_n - x_j)^2 + (y_m - y_j)^2 + (z_l \pm 3D)^2}{4Dct_d}}\right)^2\right] \cdot \left\{\left[\frac{(x_n - x_j)^2 + (y_m - y_j)^2 + (z_l \pm 3D)^2}{4Dct_d}\right]^{-1/2}\right.$$

$$+ 2\left[\frac{(x_n - x_i)^2 + (y_m - y_i)^2 + z_l^2}{4Dct_d}\right]^{-1/2} + \frac{1}{2}\left[\frac{(x_n - x_i)^2 + (y_m - y_i)^2 + z_l^2}{4Dct_d}\right]^{-3/2}$$

$$\left.+ \left[\frac{(x_n - x_i)^2 + (y_m - y_i)^2 + z_l^2}{4Dct_d}\right]^{-1} \cdot \left[\frac{(x_n - x_j)^2 + (y_m - y_j)^2 + (z_l \pm 3D)^2}{4Dct_d}\right]^{1/2}\right\}.$$

**[1] A.B. Konovalov et al.** *Proc. 7th Int. Symp. TPB-19,* **46-47 (2019)**

The reconstruction problem setup

Let $\{g_{i,j}\}_{1,1}^{I,J}$ be a known array of measurement data, where I and J are the numbers of receivers and sources used for reconstruction. Let us organize all measurement data into a vector $\mathbf{g}$ of length $K = I \times J$, all unknown discrete values of $\{\mu_{m,n,l}\}_{1,1,1}^{M,N,L}$ into a vector $\boldsymbol{\mu}$ of length $R = M \times N \times L$, and all weight coefficients $\{W_{m,n,l}^{i,j}\}_{1,1,1,1,1}^{I,J,M,N,L}$ into a sensitivity matrix $\mathbf{W}$ of size $K \times R$. Then the EP-FMT inverse problem reduces to finding a solution for an unknown vector $\boldsymbol{\mu}$ from the system of linear algebraic equations

$$\mathbf{W}\boldsymbol{\mu} = \mathbf{g}.$$

[1] A.B. Konovalov et al. *Proc. 7th Int. Symp. TPB-19,* 46-47 (2019)

The numerical phantoms we study

The scattering objects shaped as boxes have two spherical fluorescent inclusions forming the periodical structures. The diameters of inclusions are **0.5, 0.2, and 0.1 mm**. The depths are **3 and 6 mm.**

full phantom

enlarged 3D fragment
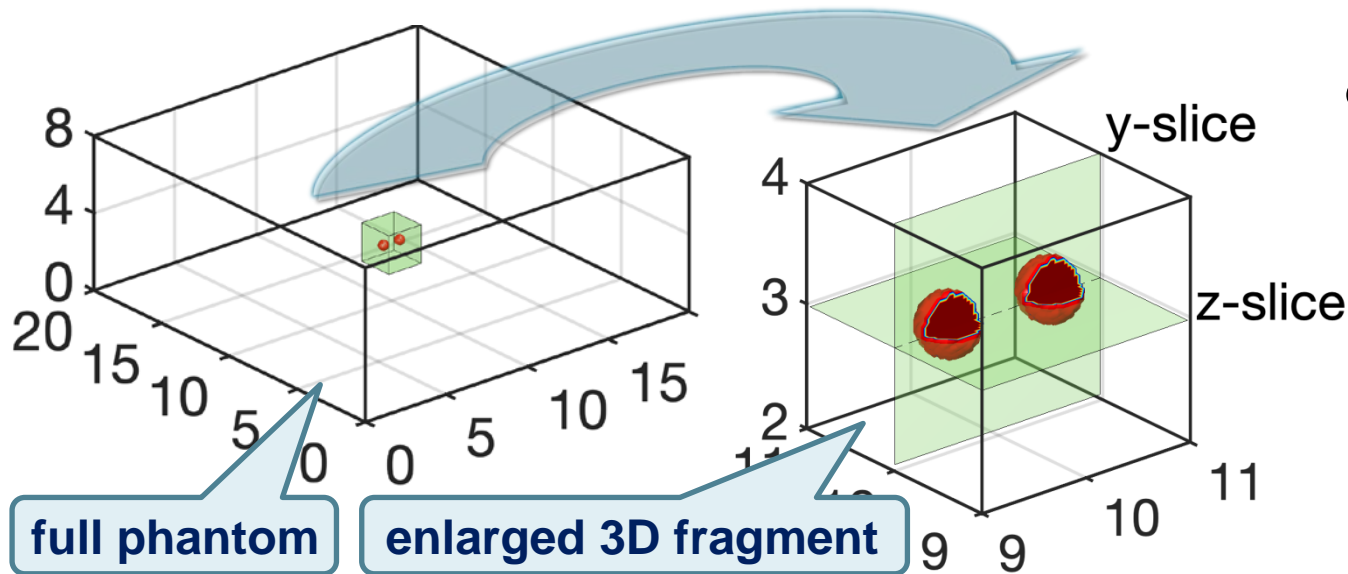
$$c = 0.214 \text{ mm} / \text{ps}$$
$$D = 0.194 \text{ mm}$$
$$\gamma = 1$$
$$\tau = 1000 \text{ ps}$$
$$\mu_{af} = 0.01 \text{ mm}^{-1}$$

For modeling the measurement data, we use the well-known software package **NIRFAST** **[2]**. The values of time gates are **100 and 150 ps**. They correspond to the SR links of **8 and 10 mm**, respectively.

[2] H. Dehghani et al. *Commun. Numer. Meth. Eng.* 25(6): 711-732 (2009)

11

Our reconstruction algorithms

❑ **We study and compare two algebraic-reconstruction-based CS algorithms.**

➤ **Algorithm 1: the algebraic reconstruction technique (ART) with total variation (TV) regularization, ART-TV**

> [3] H. Yu & G. Wang. *Phys. Med. Biol.* 54(9): 2791-2805 (2009)
>
> [4] V.V. Vlasov et al. *J. Electron. Imaging* 27(4): 043006 (2018)

➤ **Algorithm 2: the ART with fast iterative shrinkage thresholding (FIST), ART-FIST, which is our modification of the well-known fast iterative shrinkage thresholding algorithm (FISTA)**

> [5] A. Beck & M. Teboulle. *SIAM J. Imaging Sci.* 2(1): 183-202 (2009)

ART-TV: description (Slide 1)

❑ **ART-TV states and solves the optimization problem**

$$\| \mu \|_{TV} \to \min \quad \text{subject to} \quad \| \mathbf{W}\mu - \mathbf{g} \|_2 \leq \sigma, \quad \text{where} \tag{1}$$

$\| \cdot \|_{TV}$ **is the TV-norm,** $\| \cdot \|_2$ **is the** *L₂* **or Euclidean norm,**

σ **is the parameter that describes the noise level.**

❑ **Problem (1) is solved implicitly in two steps. In the first step (ART-step), the standard ART with** S_{art} **iterations is used to reconstruct the image approximation** $\mu^{(S_{art})}$ **by the formula**

$$\mu_r^{(s_{art}+1)} = \mu_r^{(s_{art})} + \lambda \frac{g_k - \sum_{r=1}^{R} W_{kr} \mu_r^{(s_{art})}}{\sum_{r=1}^{R} (W_{kr})^2} W_{kr}, \quad \text{where} \tag{2}$$

λ **is the control parameter .**

[3] H. Yu & G. Wang. *Phys. Med. Biol.* 54(9): 2791-2805 (2009)

13

ART-TV: description (Slide 2)

❑ The **second step** (**TV-step**) involves implicit minimization of the TV-norm of the image $\boldsymbol{\mu}^{(S_{art})}$ with the standard **steepest descent algorithm** which preforms S_{tv} gradient iterations by the formula

$$\mu_r^{(S_{art},s_{tv}+1)} = \mu_r^{(S_{art},s_{tv})} - \alpha \frac{\partial \| \boldsymbol{\mu}^{(S_{art},s_{tv})} \|_{TV}}{\partial \mu_r} , \quad \text{where}$$

α is the iteration step.

❑ The TV-norm and its gradient are calculated using the formulas of the **smoothed isotropic ART-TV version** which is in rather detail described in **[6]**.

❑ Then a cycle of external iterations is organized, where the **ART-** and **TV- steps** successively alternate.

[6] A.B. Konovalov & V.V. Vlasov *Proc. SPIE* 9917: 99170S (2016)

ART-FIST: description (Slide 1)

❑ **ART-FIST states and solves the optimization problem**

$$\| \boldsymbol{\mu} \|_1 \to \min \quad \textbf{subject to} \quad \| \mathbf{W}\boldsymbol{\mu} - \mathbf{g} \|_2 \leq \sigma, \quad \textbf{where} \tag{3}$$

$\| \cdot \|_1$ **is the L_1 or Manhattan norm.**

❑ **Problem (3) is solved by the Lagrange method in two steps. In the first step (ART-step), the ART with K iterations is used to reconstruct the image approximation $\boldsymbol{\mu}^{(K)}$ by formula (2), where all working SR links are gone over once.**

❑ **In the second step (shrink-step), the shrinkage thresholding operator is applied to "shrink" the image $\boldsymbol{\mu}^{(K)}$**

[5] A. Beck & M. Teboulle. *SIAM J. Imaging Sci.* 2(1): 183-202 (2009)

$$Shrink_{\beta\lambda}\left[\boldsymbol{\mu}^{(K)}\right] = \begin{cases} \boldsymbol{\mu}^{(K)} + \beta\lambda, & \boldsymbol{\mu}^{(K)} \leq -\beta\lambda \\ 0, & |\boldsymbol{\mu}^{(K)}| < \beta\lambda \\ \boldsymbol{\mu}^{(K)} - \beta\lambda, & \boldsymbol{\mu}^{(K)} \geq \beta\lambda \end{cases}, \quad \text{where}$$

β **is the regularization parameter.**

❑ **Then a cycle of external iterations is organized, where the ART- and shrink- steps successively alternate.**

❑ **The feature of ART-FIST is the acceleration procedure, where the $(s+1)-$ approximation $\boldsymbol{\mu}^{(s+1)}$ is calculated as a linear combination of $\boldsymbol{\mu}^{(s)}$ and $\boldsymbol{\mu}^{(s-1)}$ in order to make the algorithm converge faster [5].**

[5] A. Beck & M. Teboulle. *SIAM J. Imaging Sci.* 2(1): 183-202 (2009)

Strategy for algorithm study

❑ **We first reconstruct all six phantoms with use of ART-TV and ART-FIST from ideal measurement data, i.e., measurement data free of noise.**

❑ **The best algorithm is chosen through the visual analysis of resulted reconstructions.**

❑ **Just this algorithm is then tested for resistance to noise.**

➢ **In accord with [7], about 10-20% of maximum of the typical temporal point spread function correspond to relative noise of about 3%. So, additive Gaussian noise with zero mean and relative root-mean-square deviation 3% is applied to measurement data .**

[7] F. Leblond et al. *J. Opt. Soc. Am. A* 26(6): 1444-1457 (2009)

inclusions of 0.5 mm in diameter at depth 3 mm, noise 0%

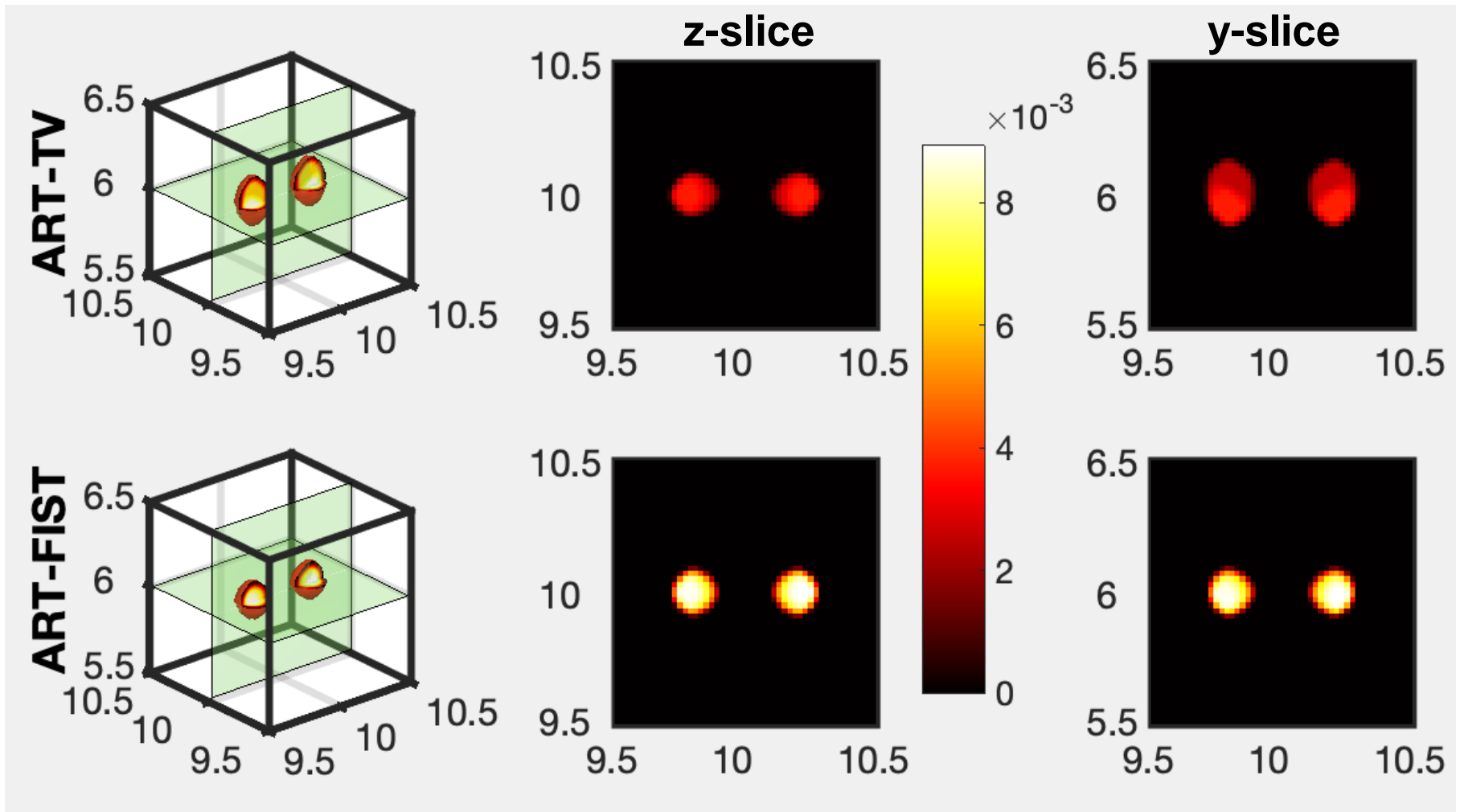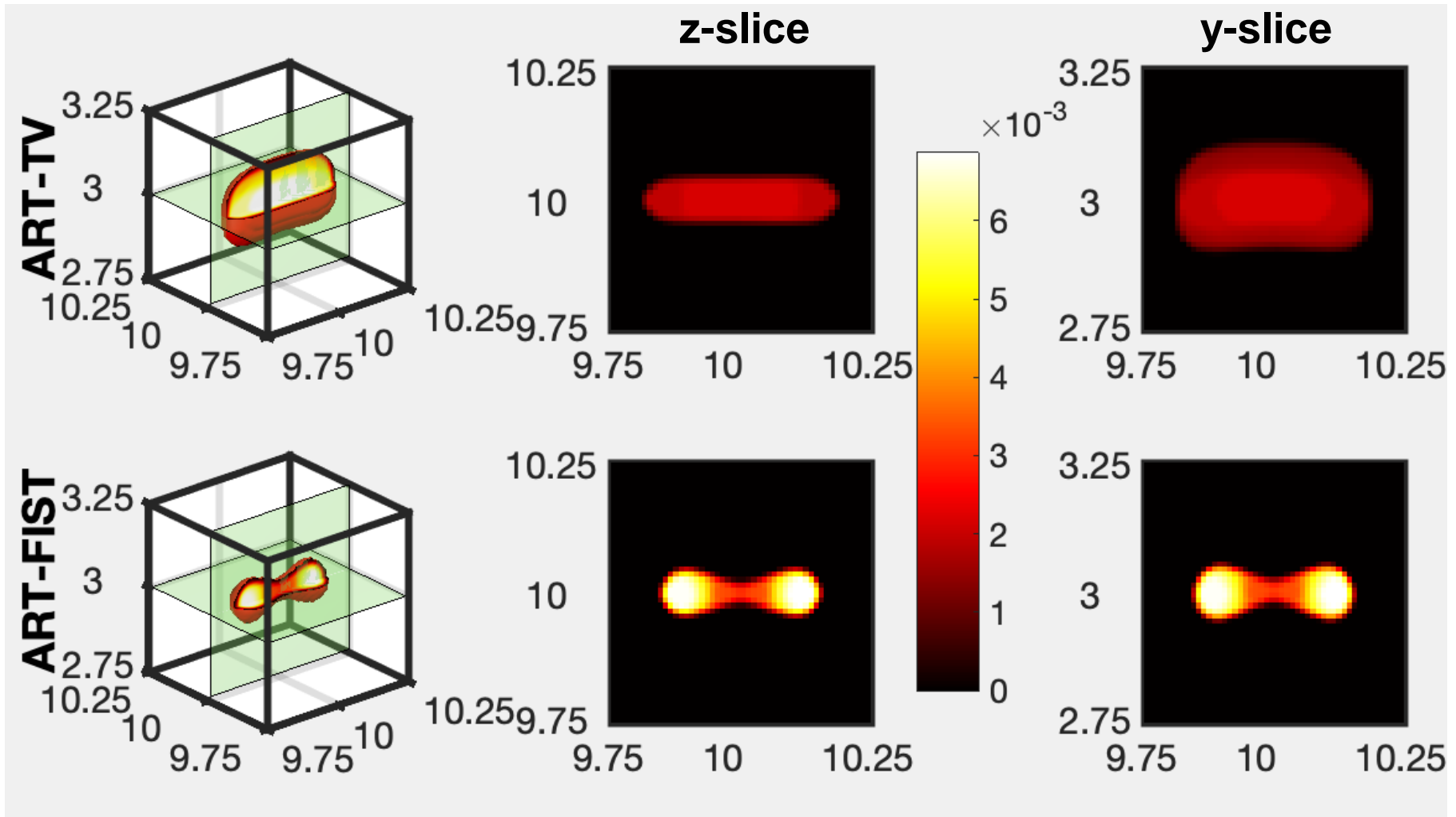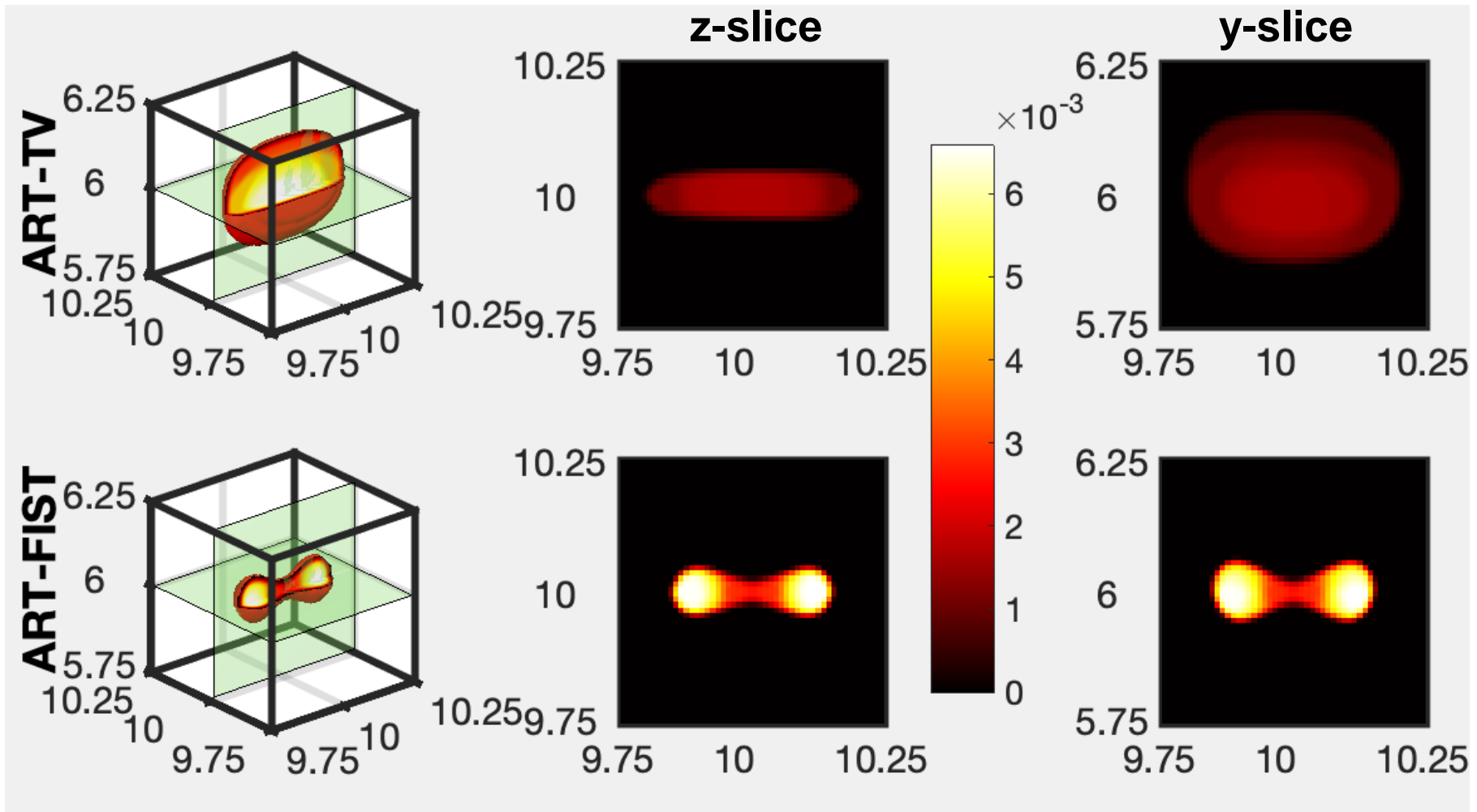**inclusions of 0.5 mm in diameter at depth 6 mm, noise 0%**
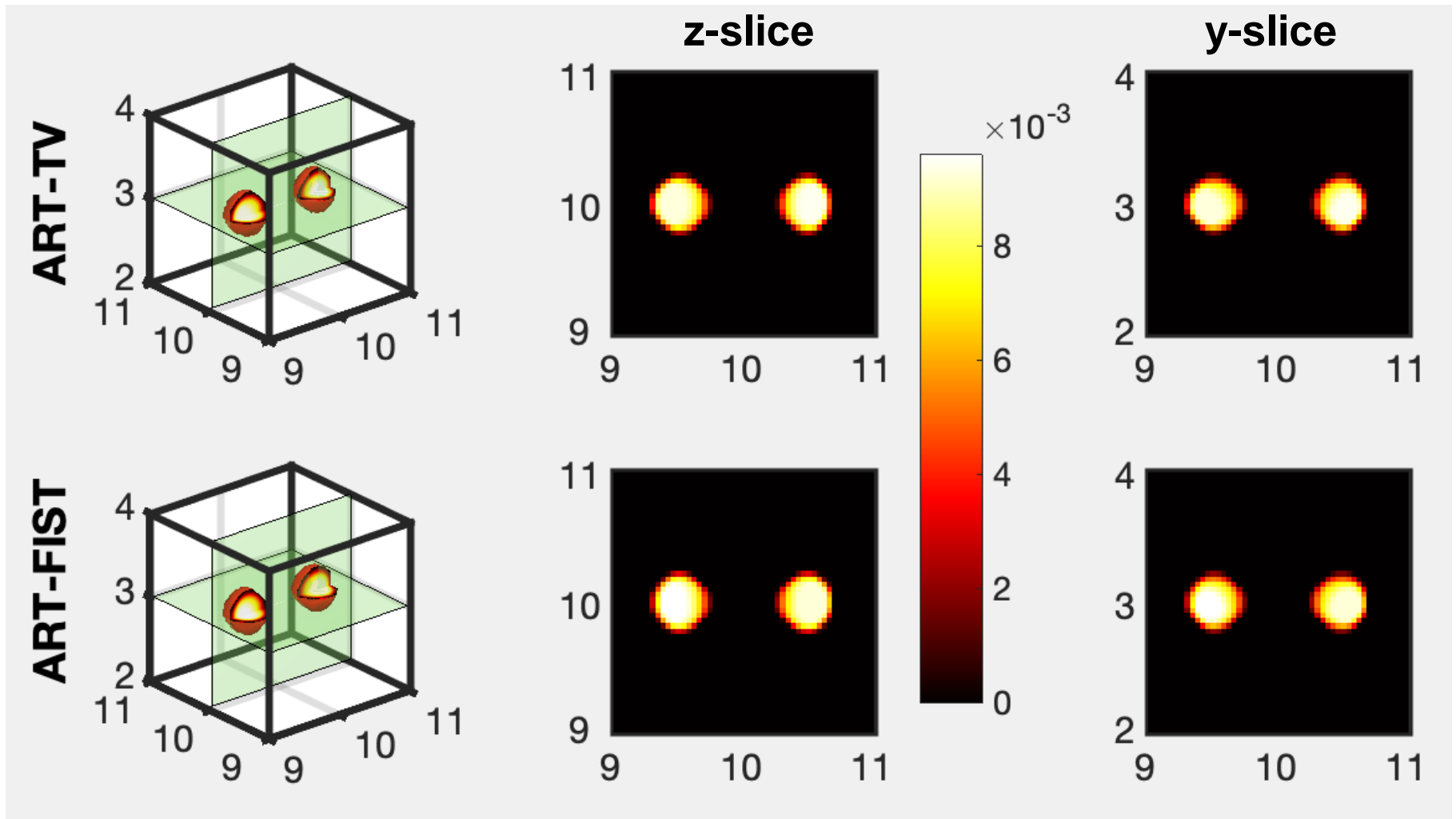
inclusions of 0.2 mm in diameter at depth 3 mm, noise 0%

Reconstruction results (Slide 4)
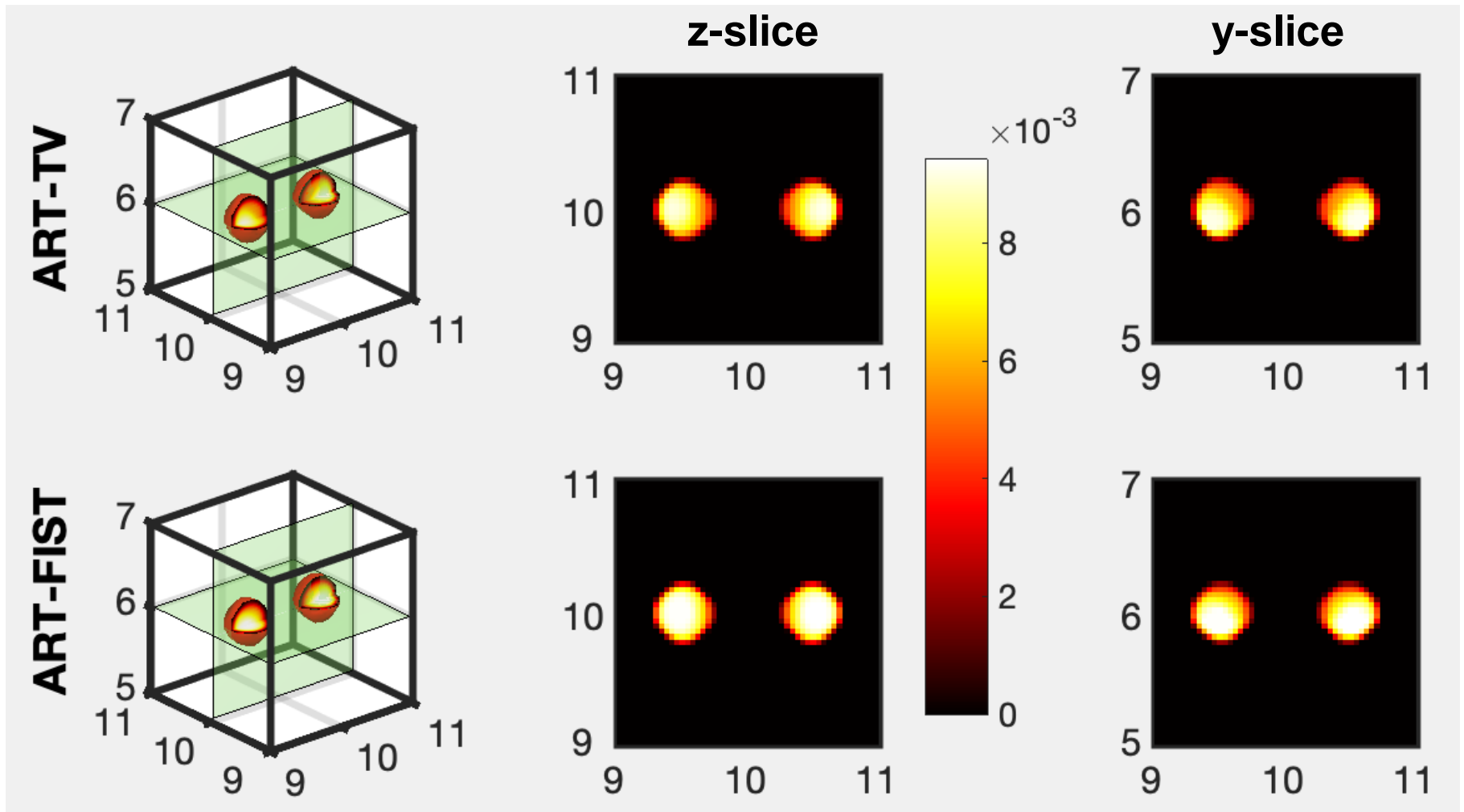
inclusions of 0.2 mm in diameter at depth 6 mm, noise 0%
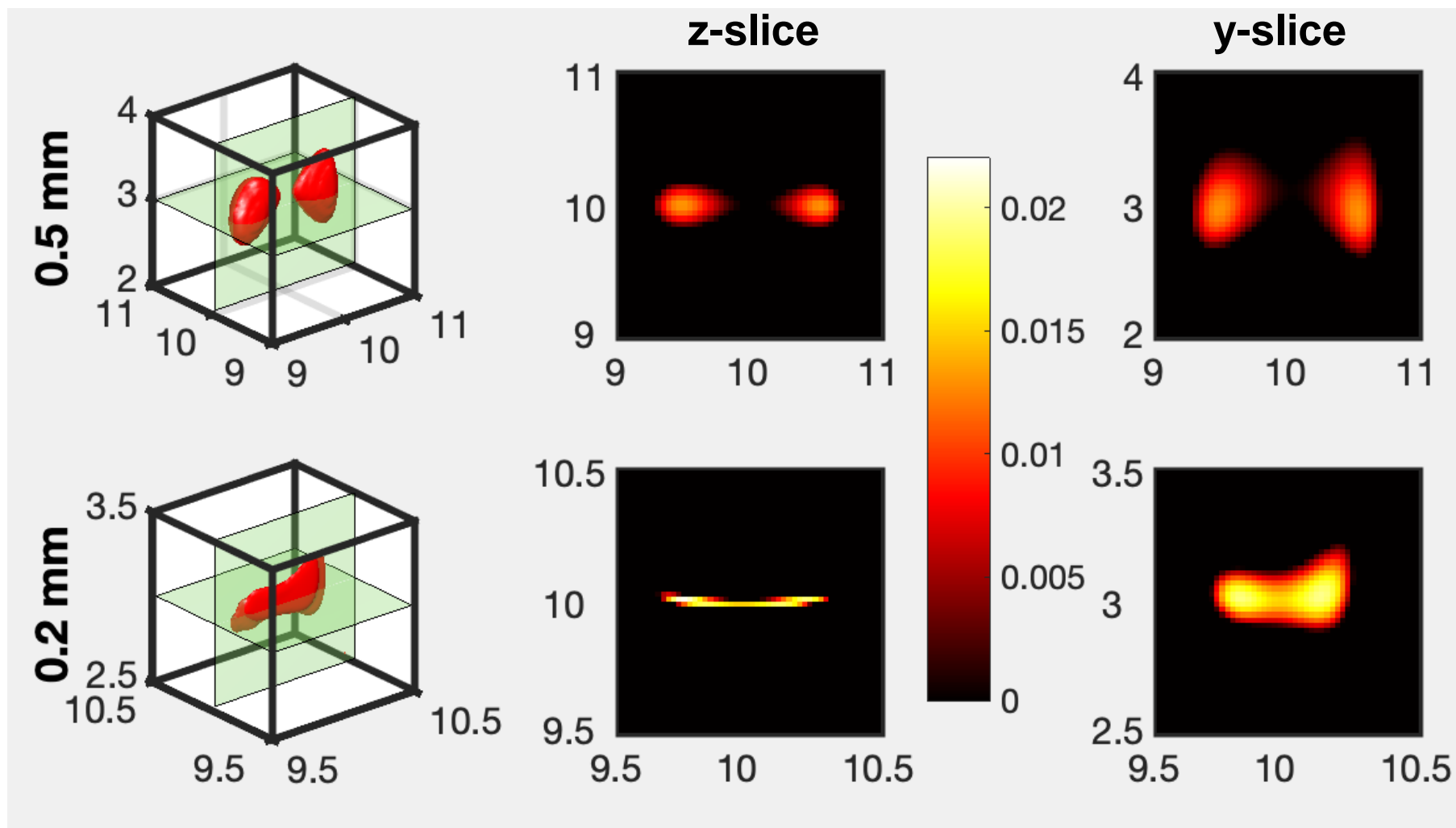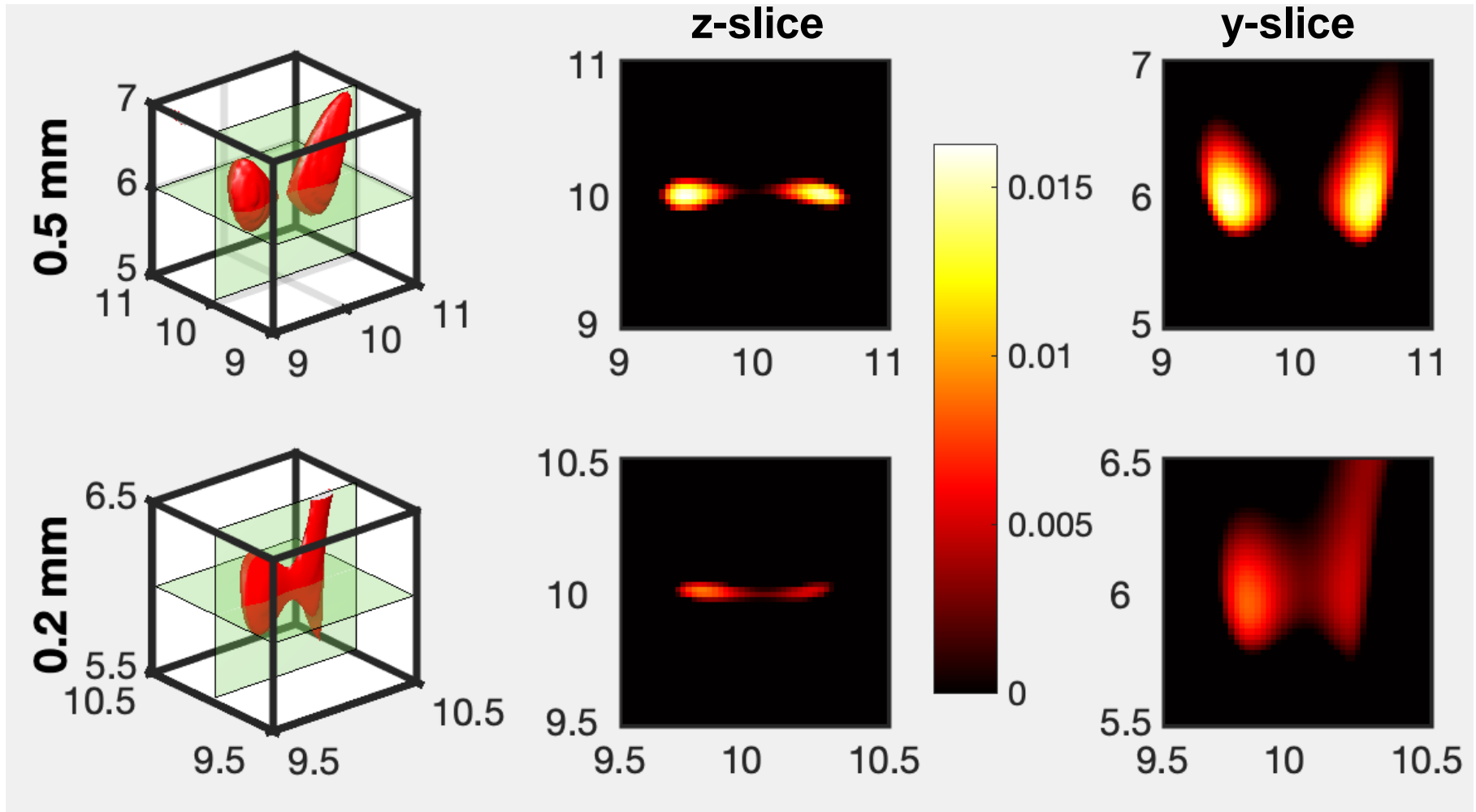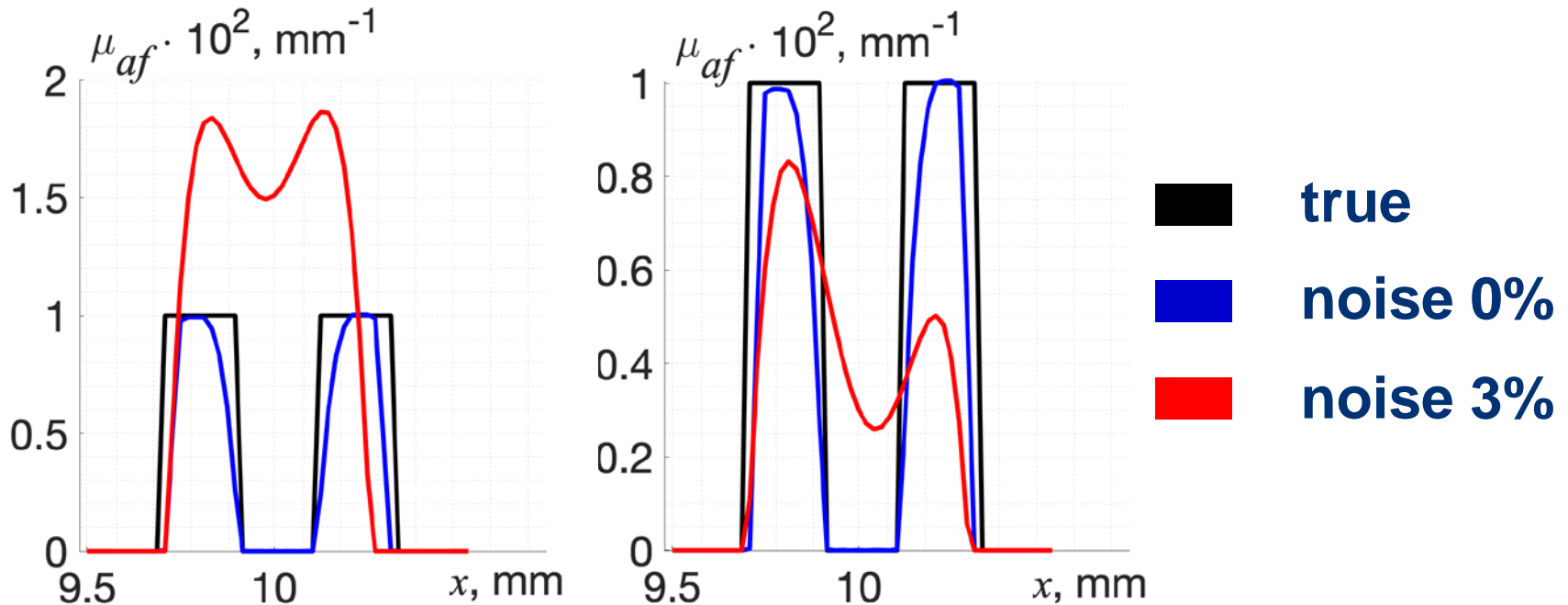
Reconstruction results (Slide 5)

RFNC-VNIITF
ROSATOM

inclusions of 0.1 mm in diameter at depth 3 mm, noise 0%

22

inclusions of 0.1 mm in diameter at depth 6 mm, noise 0%

ART-FIST, depth 3 mm, noise 3%

ART-FIST, depth 6 mm, noise 3%

Profiles for the y-slices of 3D tomograms

Legend:
- **true** (black)
- **noise 0%** (blue)
- **noise 3%** (red)

ART-FIST, inclusions 0.2 mm, depth 3 mm (left) and 6 mm (right)

❑ **The modulation transfer coefficients evaluated for the red profiles make up 20% (left) and 24% (right), respectively. This means that according to the Foucault-Rayleigh criterion, we confirm that the resolution of 0.2 mm is achievable if relative noise in measurement data is no higher than ~3%.**

Conclusions

❑ From ideal measurement data **ART-FIST** reproduces fine structures (fluorescent inclusions of **0.2 and 0.1 mm** in size) much more accurately than **ART-TV**.

❑ If measurement data are not free of noise, **ART-FIST** excellently reproduces the inclusions of 0.5 mm but has some problems with reproducing the fine structures.

❑ Nevertheless, the results show that our **EP-FMT** method with **ART-FIST** is capable of achieving as good spatial resolution as **0.2 mm** at depths to 6 mm inclusive. Given that this resolution is very close to that of **mesoscopic FMT**, our result **can be thought as quite satisfactory**.

Acknowledgement

RFNC-VNIITF
ROSATOM

We are very thankful to professor Savitsky and professor Tuchin for useful discussions of the new data registration geometry.

ABK: a_konov@mail.vega-int.ru
VVV: vitally.vlasov.v@yandex.ru
ASU: a.s.uglov@vniitf.ru

75 ЛЕТ
АТОМНОЙ
ПРОМЫШЛЕННОСТИ

ОПЕРЕЖАЯ
ВРЕМЯ

РФЯЦ-ВНИИТФ